Available online at www.sciencedirect.com
SCIENCE DIRECT®
International Journal of Heat and Mass Transfer 47 (2004) 2161–2172
International Journal of HEAT and MASS TRANSFER
www.elsevier.com/locate/ijhmt

An investigation of turbulent oscillatory heat transfer in channel flows by large eddy simulation

Lei Wang, Xi-Yun Lu *

Department of Modern Mechanics, University of Science and Technology of China, Hefei, Anhui 230026, China

Received 5 June 2003; received in revised form 22 November 2003

Abstract

Oscillating turbulent channel flow with heat transfer has been investigated by use of large eddy simulation (LES) technique. Three-dimensional filtered Navier–Stokes and energy equations are numerically solved by fractional-step method. Dynamic subgrid-scale (SGS) models for the turbulent SGS stresses and heat fluxes are employed to closure the governing equations. The objective of this study is to examine the reliability of the LES technique for predicting the turbulent oscillatory heat transfer and to analyze the behavior of turbulent heat diffusion from a solid boundary to the adjacent oscillatory shear flow. In this study, oscillating turbulent channel flow with a constant difference of temperature imposed on both the walls is calculated for the Prandtl number (Pr) from 0.1 up to 100 and the Reynolds number (Re_τ) 350 based on the friction velocity and the half-width of the channel. The frequency of driving pressure gradient for the oscillating turbulent channel flow ranges low, medium and high values. Some typical turbulence statistical quantities and structures of velocity and temperature fluctuations are analyzed.

Keywords: Large eddy simulation (LES); Oscillatory heat transfer; Turbulent channel flow; Thermal turbulence; Subgrid-scale (SGS) model

1. Introduction

Understanding and prediction of heat transfer between solid wall and adjacent turbulent fluid flow are of great interest in both applications and fundamentals. Meanwhile, inherent unsteadiness of the driving conditions (e.g., time-varying driving pressure gradient) characterizes a variety of turbulent flows. Statistically unsteady turbulent flows have received relatively little attention compared to steady ones. To the best of our knowledge, very few results concerning the effects of the Prandtl number on the heat transfer in statistically unsteady turbulent flows were reported.

In the problem of heat transfer by fluid flow, the Prandtl number can be ranged from order of unity or less to hundreds. In the case of the heat transfer at low or moderate Prandtl number, a significant temperature gradient exists not only in the diffusive sublayer but also in the region outside the sublayer. High-Prandtl number heat transfer is of special importance in the understanding of the heat transfer in a turbulent boundary layer flow. The heat diffusive sublayer for the high-Prandtl number heat transfer by the rigid boundary is very thin, and the heat transfer efficiency is primarily controlled by turbulent motions very closing to the wall. The complexity of turbulence interactions near the wall results in unusual behaviors of temperature fluctuations. Thus it is a challenging task to study the heat transfer at high-Prandtl number.

As well known, direct numerical simulation (DNS) approach can be used to calculate and analyze the temperature and velocity fluctuations near the wall. However, due to the expensive cost of DNS, previous work only limited their investigations to low- or medium-Prandtl number (usually $Pr \leqslant 10$) flow [1–7]. In fact, it is obviously impossible at the present time to use DNS approach to solve problems in which both the Reynolds

* Corresponding author. Tel.: +86-551-3603223/3601542; fax: +86-551-3606459.
E-mail address: xlu@ustc.edu.cn (X.-Y. Lu).

0017-9310/$ - see front matter © 2003 Elsevier Ltd. All rights reserved.
doi:10.1016/j.ijheatmasstransfer.2003.11.010

Nomenclature

A_P	amplitude of driving pressure gradient
C	SGS model coefficient
K_{T}^{+}	mean turbulent heat transfer coefficient
K_{TP}^{+}	phase-averaged turbulent heat transfer coefficient
$\bar{p}$	resolved modified pressure
Pr	Prandtl number
Pr_{T}	turbulent Prandtl number
q_i	SGS turbulent heat flux
Re	Reynolds number
Re_τ	Reynolds number based on the friction velocity
R_{kk}	trace of SGS Reynolds stress
$\overline{S}_{ij}$	resolved strain rate tensor
t	time
t_P	period of driving pressure gradient
$\overline{T}$	resolved temperature
T'	resolved temperature fluctuation
T^+	resolved temperature normalized by the friction temperature
T_δ	temperature on the upper wall
$T_{-\delta}$	temperature on the bottom wall
T_τ	friction temperature
u	resolved streamwise velocity component
$\bar{u}_i$	resolved velocity components
u_i'	resolved velocity fluctuations
u_τ	friction velocity
v	resolved spanwise velocity component
w	resolved wall-normal velocity component
x_i	Cartesian coordinate axes
z	wall-normal coordinate
z^+	wall-normal coordinate normalized by the friction velocity
δ	half-width of the channel
δ_{i1}	delta function along the streamwise direction
δ_{T}^{+}	thickness of diffusive sublayer
$\overline{\Delta}$	size of grid filter
$\hat{\overline{\Delta}}$	size of test filter
ω_P	frequency of driving pressure gradient
τ_{ij}	SGS turbulent stress tensor
ν	molecular kinematic viscosity
κ	thermal diffusivity
$\langle\ \rangle$	average in the whole time and in the plane parallel to the wall plate
$\langle\ \rangle_P$	phase-average at the same phase and space-average in the plane parallel to the wall plate
$\langle\ \rangle_S$	average in the plane parallel to the wall plate

Subscripts

rms	root mean square
min	minimum

Superscript

+	normalized quantity by wall parameters

and Prandtl numbers are large, since the number of mesh points required to describe all the scales is of order $Pr^3 Re^{9/4}$. However, it is now well established that large eddy simulation (LES) technique, which is much cheaper than the DNS since it solves only the large-scale components of turbulent flow and models the subgrid-scales (SGS) effects via SGS models, provides an effective tool to study detailed features of turbulent flows. Usually, the SGS model is a key problem in the LES and a dynamic SGS model was proposed by Germano et al. [8] which overcame some shortcomings of the Smagorinsky model [9]. The dynamic model gained a remarkable success in the past decade and it gave a new impetus to the development of new strategies for LES [10–15]. On account of the improvements made by the new SGS models, it becomes highly tempting to use the dynamic SGS model for studying the turbulent heat transfer at high-Prandtl number.

On the other hand, statistically unsteady turbulent flows driven by time-varying external force have received very little attention compared to statistically steady ones. Spalart and Baldwin [16] carried out the DNS of a turbulent oscillating boundary layer and dealt with the transition problem in the purely oscillating flow. Lu et al. [17] performed the LES for an oscillating turbulent flow past a circular cylinder. Then, Hsu et al. [18] first employed the LES technique coupled with dynamic SGS model to investigate an oscillating turbulent flow over a plate and confirmed that the LES approach based on the dynamic SGS model is suited to tackle unsteady problems. Recently, Scotti and Piomelli [19] carried out the LES of pulsating turbulent channel flow driven by an oscillating pressure gradient and verified that the LES approach can predict reasonably unsteady turbulent behavior.

In this paper, LES technique is employed to investigate oscillating turbulent channel flow with heat transfer. To authors' knowledge, it is the first time to study the problem, in particular for high-Prandtl number heat transfer, by use of the LES approach. The oscillating turbulent channel flow driven by a time-varying pressure gradient with constant difference of temperature imposed on different walls is calculated. Three-dimensional resolved incompressible Navier–Stokes equations are solved by the fractional-step method proposed by Verzicco and Orlandi [20]. Dynamic SGS models for SGS

turbulent stresses and turbulent heat fluxes are employed to closure the equations.

2. Mathematical formulations

To investigate turbulent oscillatory heat transfer in a channel flow, the three-dimensional, time-dependent filtered incompressible Navier–Stokes and energy equations are simultaneously solved. To non-dimensionalize these equations, the half-width of the channel δ is used as the length scale, the mean friction velocity u_τ, which will be defined in the following, as the velocity scale, and the difference of temperature between the upper and lower walls ΔT as the temperature scale. Then, the non-dimensional governing equations are given as

$$\frac{\partial \bar{u}_i}{\partial x_i} = 0 \tag{1}$$

$$\frac{\partial \bar{u}_i}{\partial t} + \frac{\partial}{\partial x_j}(\bar{u}_i \bar{u}_j) = -\frac{\partial \bar{p}}{\partial x_i} + \frac{1}{Re_\tau}\frac{\partial^2 \bar{u}_i}{\partial x_j \partial x_j} - \frac{\partial \tau_{ij}}{\partial x_j} + P_g \delta_{i1} \tag{2}$$

$$\frac{\partial \overline{T}}{\partial t} + \frac{\partial (\overline{T}\bar{u}_j)}{\partial x_j} = \frac{1}{Re_\tau Pr}\frac{\partial^2 \overline{T}}{\partial x_j \partial x_j} - \frac{\partial q_j}{\partial x_j} \tag{3}$$

where $\tau_{ij} = R_{ij} - \delta_{ij}R_{kk}/3$, $R_{ij} = \overline{u_i u_j} - \bar{u}_i \bar{u}_j$, $q_j = \overline{Tu}_j - \overline{T}\bar{u}_j$, overbar "–" represents the resolved variable, the Reynolds number Re_τ is defined as $Re_\tau = u_\tau \delta/\nu$, and the Prandtl number Pr as $Pr = \nu/\kappa$ with ν being the kinematic viscosity and κ the thermal diffusivity of the fluid. $\bar{u}_i$ and $\overline{T}$ are the resolved velocity and temperature. Here, the resolved velocity $\bar{u}_i$ $(i = 1, 2, 3)$, for writing convenience, is represented as u, v and w in the streamwise (x), spanwise (y) and wall-normal (z) directions, respectively. $\bar{p}$ is the resolved modified pressure, which contains a term $R_{kk}/3$. $P_g \delta_{i1}$ denotes an external pressure gradient along the streamwise direction, and the pressure gradient P_g represents

$$P_g = 1 + A_P \cos(\omega_P t) \tag{4}$$

where $\omega_P = 2\pi/t_P$, and A_P, ω_P and t_P denote the amplitude, frequency and period of oscillating pressure gradient, respectively. Then, as used by Scotti and Piomelli [19], the friction velocity u_τ is defined based on the mean part of the pressure gradient in Eq. (4).

In Eqs. (2) and (3), τ_{ij} and q_j represent SGS turbulent stress and heat flux, respectively, which need to be modeled by SGS models. It is assumed that the heat transfer is a passive scalar that does not influence the flow dynamics. Thus the temperature depends on both Re_τ and Pr independently. The overall expressions of the SGS stresses and turbulent heat flux are given as

$$\tau_{ij} = -2C\bar{\Delta}^2 |\overline{S}| \overline{S}_{ij}, \quad q_j = -\frac{C\bar{\Delta}^2}{Pr_T}|\overline{S}|\frac{\partial \overline{T}}{\partial x_j} \tag{5}$$

where $\overline{S}_{ij} = (\partial \bar{u}_i/\partial x_j + \partial \bar{u}_j/\partial x_i)/2$, $|\overline{S}| = [2\overline{S}_{ij}\overline{S}_{ij}]^{1/2}$. $\bar{\Delta}$ is the filter width, and Pr_T represents the turbulent Prandtl number.

The model coefficients of C and Pr_T in Eq. (5) are obtained by the approach proposed by Germano et al. [8]. After introducing a test filtering with a filter width $\hat{\bar{\Delta}}$ to Eqs. (1)–(3), the coefficients C and Pr_T can be dynamically determined, by a least-square approach, as

$$C = -\frac{1}{\bar{\Delta}^2}\frac{\langle L_{ij}M_{ij}\rangle_S}{\langle M_{ij}M_{ij}\rangle_S}, \quad Pr_T = -C\bar{\Delta}^2\frac{\langle F_i F_i\rangle_S}{\langle H_i F_i\rangle_S} \tag{6}$$

where

$$M_{ij} = 2\alpha^2|\hat{\overline{S}}|\left[\hat{\overline{S}}_{ij} - \tfrac{1}{3}\hat{\overline{S}}_{kk}\delta_{ij}\right] - \hat{m}_{ij},$$

$$L_{ij} = \hat{\bar{u}_i}\hat{\bar{u}_j} - \hat{\bar{u}}_i\hat{\bar{u}}_j - \tfrac{1}{3}(\hat{\bar{u}_k}\hat{\bar{u}_k} - \hat{\bar{u}}_k\hat{\bar{u}}_k)\delta_{ij},$$

$$m_{ij} = 2|\overline{S}|\left[\overline{S}_{ij} - \tfrac{1}{3}\overline{S}_{kk}\delta_{ij}\right], \quad E_i = \hat{\bar{u}}_i\hat{\overline{T}} - \hat{\bar{u}_i\overline{T}},$$

$$F_i = \alpha^2|\hat{\overline{S}}|\hat{\bar{B}}_i - \hat{|\overline{S}|B_i} \quad \text{and} \quad B_j = \frac{\partial \overline{T}}{\partial x_j}$$

Here, $\alpha = \hat{\bar{\Delta}}/\bar{\Delta}$ is chosen as 2 in the present calculation, $\langle\ \rangle_S$ denotes some kind of spatial averaging to remove the calculation oscillation [8]. It is still needed to note that the validity of the dynamic SGS models to study this kind of unsteady turbulent flow has been established [17–19].

In this study, no-slip and no-penetration velocity conditions are imposed at both the channel walls $z = \pm 1$. The flow and temperature fields are assumed to be statistically homogeneous in the streamwise and spanwise directions. Thus, periodic boundary conditions are employed in those directions. Two different constant temperatures $T_\delta = 0.5$ and $T_{-\delta} = -0.5$ are imposed on the top and bottom walls, which drive the heat transfer. Initial temperature field is set to be a linear distribution along the z-direction and homogeneous in the horizontal planes. Heat transfer computation is started after the flow field has statistically reached a fully developed turbulent state.

3. Numerical methods

To perform LES calculation, a fractional-step method developed by Verzicco and Orlandi [20] is employed to solve Eqs. (1)–(3). Spatial derivatives are discretized by a second order central difference. Time advancement is carried out by the semi-implicit scheme using the Crank–Nicolson scheme for the viscous terms and the three-stage Runge–Kutta scheme for the convective terms. The discretized formulation was described in detail by Verzicco and Orlandi [20].

In this study, the size of computational domain is $3\pi\delta \times 4\pi\delta/3 \times 2\delta$ with the corresponding grid number $97 \times 97 \times 97$ in the streamwise, spanwise and wall-normal

directions, respectively. The domain size is chosen such that two-point correlations in both the streamwise and spanwise directions are negligibly small. The grid independence of the present calculation has been ensured for each simulation. The grid is uniform along the streamwise and spanwise directions. As well known, in a wall bounded flow, the resolution for resolving the viscous sublayer near the wall is a critical problem in LES [21]. Thus, to increase the grid resolution near both the walls in the wall-normal direction, the mesh is stretched following the transformation used in [15,22], so that the grid distribution in the z-direction is sufficient to resolve the viscous sublayer and diffusive sublayer near the boundary.

To validate quantitatively the present calculation, some typical DNS results of Na et al. [7] are used to examine our calculated results. Here, two cases with $Re_\tau = 150$ and $Pr = 1$ and 10, which were studied by Na et al. [7] using DNS, are investigated. The distributions of mean temperature are shown in Fig. 1a. It is seen that our calculated result is in good agreement with the DNS data. Moreover, we have compared other turbulent quantities with some typical previous DNS results (not shown here) and can confirm that our calculation code enables the LES results to be satisfactory. To demonstrate that the computed results are independent of the time steps and grid sizes, the results calculated by different grid numbers and time steps are also shown in Fig. 1a.

Further, to exhibit the performance of the present LES at high-Prandtl number, a typical case is considered for a fully developed turbulent channel flow with a passive heat transfer at $Pr = 100$ and $Re = 10^4$ based on the mean velocity and the half-width of the channel. Fig. 1b shows the profile of mean temperature normalized by the friction temperature. Experimental and computational data given by Nagano and Shimada [23] at $Pr = 95$ with the same Reynolds number are depicted in Fig. 1b. Although the Prandtl number in this calculation is somewhat different from that in [23], both the results are reasonably in good agreement with each other.

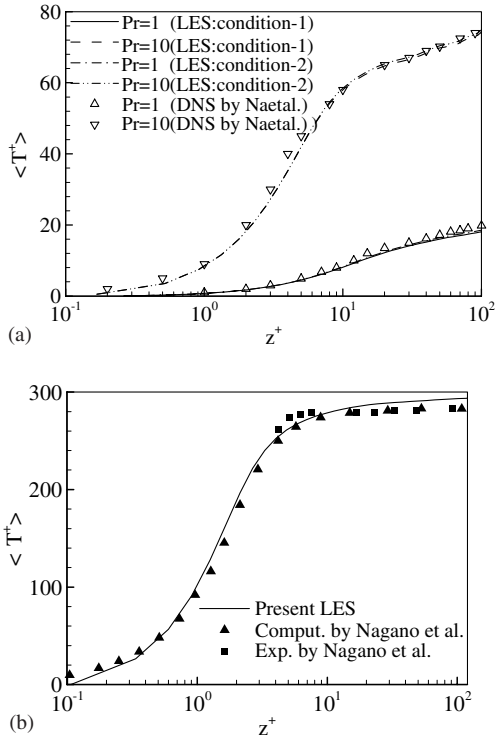

Fig. 1. Validation and verification for the present calculations: (a) mean temperature profiles for $Pr = 1$ and 10 and comparison with DNS data [7] with condition 1: grid number $65\times97\times65$ and time step 0.001 as well as condition 2: grid number $129\times193\times129$ and time step 0.0005; (b) mean temperature profile for a fully developed turbulent channel flow with a passive heat transfer at $Pr = 100$ and comparison with experimental and computational data [23].

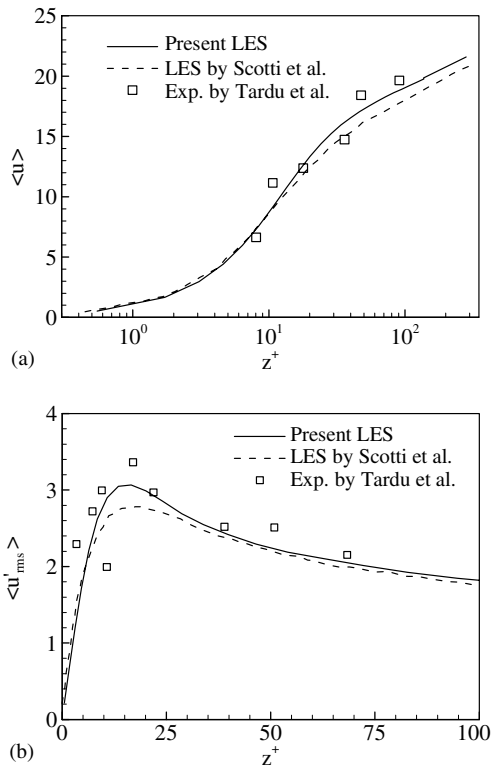

Fig. 2. Distributions of the mean streamwise velocity and its fluctuation at medium frequency (i.e., case 2), and comparison with data obtained numerically by Scotti and Piomelli [19] and experimentally by Tardu et al. [24]: (a) mean streamwise velocity; (b) mean streamwise velocity fluctuation.

4. Results and discussion

Typical calculations have been undertaken for the Prandtl number $Pr = 0.1$ to 100, and the Reynolds number $Re_\tau = 350$. The oscillating turbulent flow with the mean and the oscillating parts is driven by the pressure gradient. The amplitude (A_P) and frequency (ω_P) of the oscillating pressure gradient in Eq. (4) are given as follows: $\omega_P = 0.56$, $A_P = 8$ (hereafter, referred to as case 1); $\omega_P = 3.5$, $A_P = 50$ (case 2); and $\omega_P = 14.0$, $A_P = 200$ (case 3), which were investigated numerically by Scotti and Piomelli [19]. Three cases correspond to low, medium and high frequency with the ratio between the oscillating and mean centerline velocity approximately 0.7.

4.1. Turbulent flow characteristics

To demonstrate the mean quantities of oscillating turbulent flow, Fig. 2 shows the mean streamwise velocity (i.e., $\langle \bar{u} \rangle$) and its fluctuation (i.e., $\langle u'_{\rm rms} \rangle$) for the oscillating turbulent channel flow. It is interesting to find that there exists a buffer layer followed by a standard logarithmic region in the velocity profile, which is closely similar to that of a fully developed turbulent channel flow driven by a constant pressure gradient. To validate the present calculation further, numerical and experimental results [19,24] are shown in Fig. 2. The experimental data are consistently higher than those obtained numerically by the LES, and the present calculated results are in better agreement with the experimental data [24].

As well known, the oscillating channel flow differs significantly from the steady one. Fig. 3a shows the phase-averaged streamwise velocity (i.e., $\langle \bar{u} \rangle_P$) profiles during the cycle. Based on the velocity profiles, a layer that obeys the semi-logarithmic law exists above the viscous sublayer, especially when the centerline velocity is near its maximum. However, the semi-logarithmic law regions in the accelerating phase are narrower and closer to the wall (e.g., $0t_P/8$ and $t_P/8$), while those in the decelerating phase are broader and more far away from the wall (e.g., $3t_P/8$ and $4t_P/8$). This behavior reveals the difference in turbulence characteristics between the accelerating and decelerating phases, which was verified experimentally [25] and numerically [18].

The distributions of the phase-averaged root-mean-square values (or turbulence intensities) of the velocity fluctuations are demonstrated in Fig. 3b–d. The intensity of $\langle u'_{\rm rms} \rangle_P$ (Fig. 3b) is generally higher than those of other two components $\langle v'_{\rm rms} \rangle_P$ (Fig. 3c) and $\langle w'_{\rm rms} \rangle_P$ (Fig. 3d). The peak values of $\langle u'_{\rm rms} \rangle_P$ in the decelerating phase

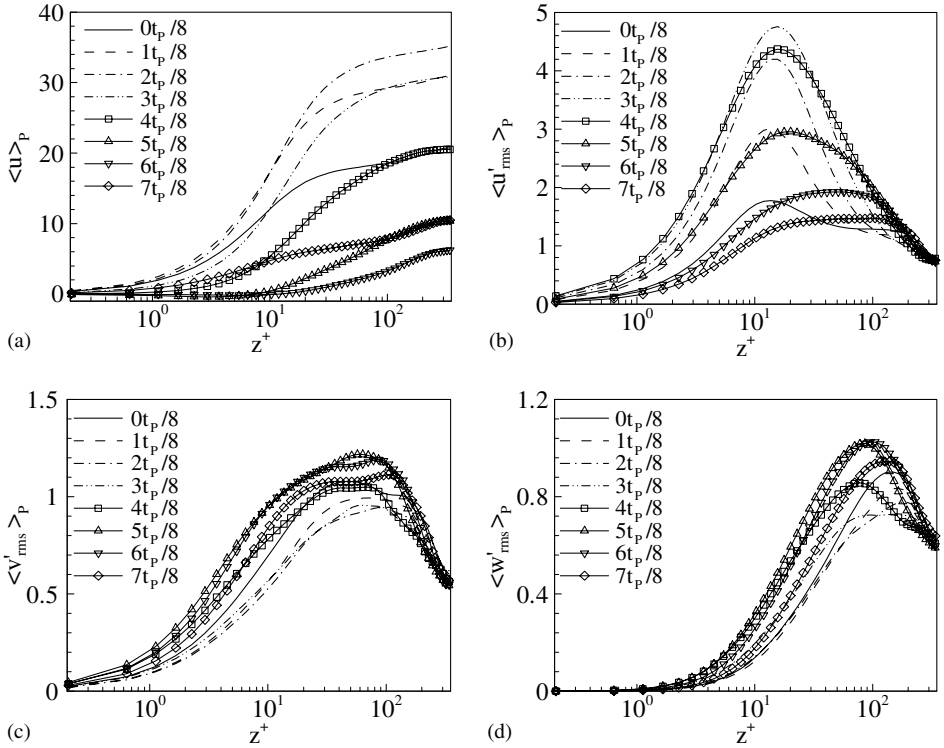

Fig. 3. Profiles of the phase-averaged streamwise velocity and velocity fluctuations at medium frequency: (a) streamwise velocity; (b) streamwise velocity fluctuation; (c) spanwise velocity fluctuation; (d) wall-normal velocity fluctuation.

are higher than those in the accelerating phase, i.e., the streamwise velocity fluctuation is mainly generated during the deceleration and suppressed during the acceleration. This behavior was confirmed experimentally [25] and numerically [18]. However, the variation of the spanwise and wall-normal intensities near the wall during the cycle has the opposite behavior with respect to the change of the streamwise intensity, and the behavior is consistent with the finding [19]. Thus, the distributions of the spanwise and wall-normal intensities near the wall at the phases from $0t_P/8$ to $3t_P/8$ exhibit obviously lower than those at the phases from $4t_P/8$ to $7t_P/8$. Further, based on the analysis of the Reynolds-stress budgets at different phases (not shown here), turbulence production characteristics during the acceleration and deceleration phases agree with the evolution of the velocity fluctuations in Fig. 3.

4.2. Turbulent heat transfer

To demonstrate the behavior of turbulent heat transfer in the vicinity of the wall, the mean temperature near the bottom wall, i.e., $\langle T^+\rangle = [\langle \overline{T}(z)\rangle - \overline{T}(-1)]/T_\tau$, is shown in Fig. 4a versus $z^+ = (z+1)u_\tau/\nu$ in logarithmic scale, where the friction temperature T_τ is defined as $T_\tau = (\kappa/u_\tau)[\partial\langle\overline{T}\rangle/\partial z]_{z=-1}$. It is seen that higher temperature appears at larger Prandtl number in the vicinity of the wall. Similar to the mean velocity distribution, there exists a buffer layer followed by a logarithmic region in the mean temperature profile, where $\langle T^+\rangle$ behaves as

$$\langle T^+\rangle = \beta_1(Pr)z^+ \quad \text{and} \quad \langle T^+\rangle = \alpha\ln z^+ + \beta_2(Pr) \tag{7}$$

where $1/\alpha$ represents the von Karman constant for the mean temperature profile, β_1 and β_2 do not vary with z^+ but change with the Prandtl number. Kader and Yaglom [26] found $\alpha = 2.12$ approximately while Kader [27] gave an empirical expression for the function β_2 that describes the experimental results in the logarithmic region of the fully turbulent boundary layer. The logarithmic curve of (7) is plotted in Fig. 4a. It is interesting to note that the slope of α is approximately constant for $Pr = 0.1$, 1, 10, 50 and 100, almost independent of the Prandtl number. This means that the z^+-logarithmic plots of mean temperature profile may be nearly parallel for different Pr numbers, which was confirmed based on DNS calculations [5,6].

Within the diffusive sublayer near the boundary, Shaw and Hanratty [28] proposed theoretically a relation between the non-dimensional thickness δ_T^+ of the heat diffusive sublayer and its dynamic equivalent δ_u^+ through the Prandtl number for statistically steady turbulent flow with heat transfer, $\delta_T^+ = Pr^{-1/3}\delta_u^+$. To illustrate the behavior of mean diffusive sublayer, based on the mean temperature profiles in Fig. 4a, it can be found that the mean diffusive boundary layer thickness gets thinner and thinner with the increase of the Prandtl

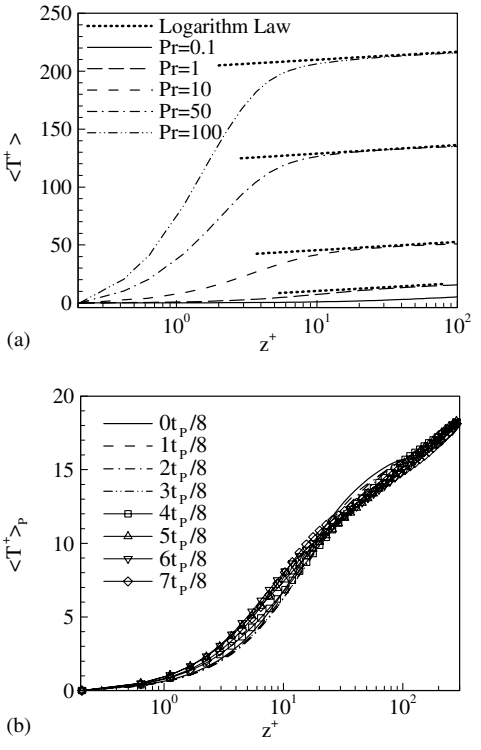

Fig. 4. Profiles of the mean and phase-averaged temperature at medium frequency: (a) mean temperature for different Prandtl numbers; (b) phase-averaged temperature for $Pr = 1$.

number. If we renormalize these profiles in the vicinity of the wall, it is easy to obtain that the values of mean diffusive sublayer thickness for different Pr numbers are related approximately by the $Pr^{-1/3}$ law given theoretically or by the $Pr^{-0.3}$ law predicted experimentally [28].

Further, the phase-averaged temperature (i.e., $\langle T^+\rangle_P = [\langle\overline{T}(z)\rangle_P - \overline{T}(-1)]/T_\tau$) profiles for $Pr = 1$ are shown in Fig. 4b. Similar to the mean temperature distribution in Fig. 4a, the buffer layer and the logarithmic region still appear approximately in the phase-averaged temperature profiles. Following the relation (7), the phase-averaged temperature, $\langle T^+\rangle_P$, can also be written as

$$\langle T^+\rangle_P = \beta_1(t/t_P, Pr)z^+ \quad \text{and}$$
$$\langle T^+\rangle_P = \alpha\ln z^+ + \beta_2(t/t_P, Pr) \tag{8}$$

where β_1 and β_2 are dependent on the Prandtl number and the phase (t/t_P) while α is still chosen as $\alpha = 2.12$ approximately found by Kader and Yaglom [26]. As expected, the slope of α is approximately constant from Fig. 4b, and almost independent of the Prandtl number and the phase.

Based on the mean and phase-averaged temperature, we discuss the Prandtl number dependence of the corresponding mean and phase-averaged turbulent heat transfer coefficients, K_T^+, K_{TP}^+, respectively, defined as

$$K_{\mathrm{T}}^{+}=\frac{\kappa}{u_{\tau}\Delta T_{\mathrm{c}}}\left(\frac{\partial\langle\overline{T}\rangle}{\partial z}\right)\Big|_{z=-1} \quad \text{and}$$

$$K_{\mathrm{TP}}^{+}=\frac{\kappa}{u_{\tau}\Delta T_{\mathrm{c}}}\left(\frac{\partial\langle\overline{T}\rangle_{P}}{\partial z}\right)\Big|_{z=-1} \tag{9}$$

where ΔT_{c} is the difference of temperature between the wall and the core of the channel flow. Kader and Yaglom [26] suggests the Pr dependence of K_{T}^{+} as $K_{\mathrm{T}}^{+}\sim Pr^{-2/3}$ as $Pr\to\infty$ for fully developed statistically steady turbulent wall flow with heat transfer. Shaw and Hanratty [28] found $K_{\mathrm{T}}^{+}\sim Pr^{-0.7}$ from their experiment. As shown in Fig. 5, it is found that the turbulent heat transfer coefficient K_{T}^{+} and K_{TP}^{+} calculated by the mean and phase-averaged quantities of the oscillatory heat transfer fall approximately between the $Pr^{-0.7}$ law predicted experimentally [28] and the $Pr^{-2/3}$ law proposed theoretically [26]. Thus, the mean and phase-averaged quantities of the oscillating turbulent flow with heat transfer still obey reasonably the relation predicted theoretically or experimentally for fully developed statistically steady turbulent wall flow with heat transfer.

Fig. 6a shows the profiles of mean temperature fluctuation (i.e., $\langle T'_{\mathrm{rms}}\rangle$) for $Pr=0.1$ to 100. Here, the temperature fluctuation is normalized by the friction temperature T_{τ} and, for writing convenience, is still denoted as T' in the following description. At $Pr=0.1$, the intensity of the fluctuating part of temperature is high all over the channel. Unlike the velocity fluctuations, the temperature intensity reaches a maximum at the central plane of the channel. According to Lyons et al. [29,30], this character is due to the fact that the different boundary conditions of the temperature imposed on different walls cause a non-zero mean temperature gradient in the center of the channel. At $Pr=1$, it is noticed that there is a local extremum in the temperature fluctuation at approximately $z^{+}=18$ from the closest channel wall, which is close to the maximum of the streamwise velocity fluctuation that occurs approximately at $z^{+}=16$, as shown in Fig. 2. As the distance from the wall goes to zero, both the fluctuations of velocity and temperature approach to zero linearly with a slope varying with the Prandtl number. At $Pr=50$ and 100, it has been shown that large temperature fluctuations are significant only close to the wall and the maximum of them shifts towards the wall as the Prandtl number increases.

The phase-averaged temperature fluctuation (i.e., $\langle T'_{\mathrm{rms}}\rangle_{P}$) for $Pr=1$ at different phases is shown in Fig. 6b.

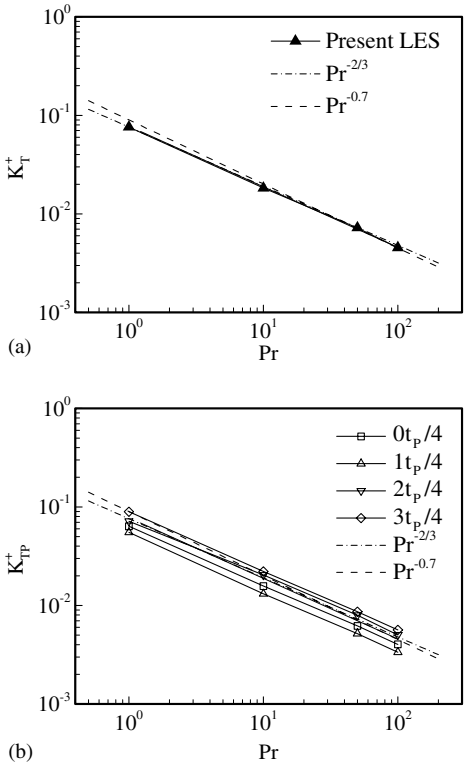

Fig. 5. Distribution of the mean and phase-averaged turbulent heat transfer coefficients versus Prandtl number at medium frequency: (a) mean turbulent heat transfer coefficient; (b) phase-averaged turbulent heat transfer coefficient.

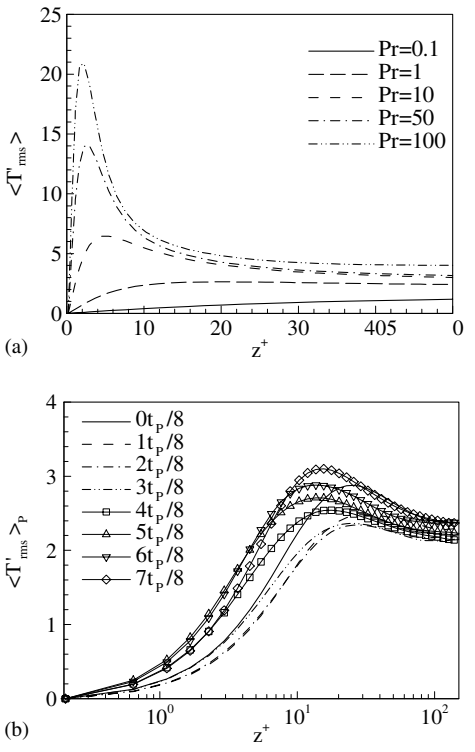

Fig. 6. Profiles of the mean and phase-averaged temperature fluctuation at medium frequency: (a) mean temperature fluctuation for different Prandtl numbers; (b) phase-averaged temperature fluctuation for $Pr=1$.

The distributions of the temperature fluctuation near the wall at the phases from $0t_P/8$ to $3t_P/8$ are obviously lower than those at the phases from $4t_P/8$ to $7t_P/8$. Because the temperature fluctuation is closely relevant to the velocity fluctuations, the variation of the temperature fluctuation is consistent with the change of the velocity fluctuations in Fig. 3.

To reveal the character of mean turbulent heat transfer near the solid walls of the oscillating turbulent channel flow, Fig. 7 shows the variations of the mean streamwise and wall-normal turbulent heat fluxes versus z^+, respectively, in the wall region for different Prandtl numbers from 0.1 to 100. As the Prandtl number increases, the heat fluxes by turbulent transport $\langle u'T'\rangle$ and $\langle w'T'\rangle$ become increasingly significant in the region near the wall. Furthermore, we can expand $\langle u'T'\rangle$ and $\langle w'T'\rangle$ into power series of z^+ in the vicinity of wall,

$$\langle u'T'\rangle = a_1 z^{+^2} + a_2 z^{+^3} + \cdots \tag{10a}$$

$$\langle w'T'\rangle = b_1 z^{+^3} + b_2 z^{+^4} + \cdots \tag{10b}$$

Here, note that $w' = c_1 z^{+^2} + c_2 z^{+^3} + \cdots$, due to $(\partial w'/\partial z)|_{z=\pm 1} = 0$.

Both curves of the square and cubic laws with the wall-normal distance are plotted in Fig. 7 with logarithmic scales to illustrate the first terms in (10). The turbulent heat fluxes in the streamwise and wall-normal directions agree well with the leading term behavior in (10) in the near wall region.

The corresponding phase-averaged streamwise and wall-normal turbulent heat fluxes (i.e., $\langle u'T'\rangle_P$ and $\langle w'T'\rangle_P$) at $Pr = 1$ during the cycle are shown in Fig. 8. The variation of the streamwise and wall-normal turbulent heat fluxes is relevant to the corresponding change of the velocity fluctuations in the streamwise and wall-normal directions. The distributions of $\langle u'T'\rangle_P$ in the decelerating phase are higher than those in the accelerating phase, i.e., the streamwise turbulent heat flux is mainly generated during the deceleration and suppressed during the acceleration. Corresponding to the development of the wall-normal velocity fluctuation in Fig. 3, the distributions of the wall-normal turbulent heat flux near the wall during the phases from $0t_P/8$ to $3t_P/8$ are lower than those during the phases from $4t_P/8$ to $7t_P/8$. Meanwhile, both curves of the square and cubic laws with the wall-normal distance are demonstrated in Fig. 8. The turbulent heat fluxes in the streamwise and wall-normal directions at different phases agree well with the leading term behavior in (10) in the near wall region.

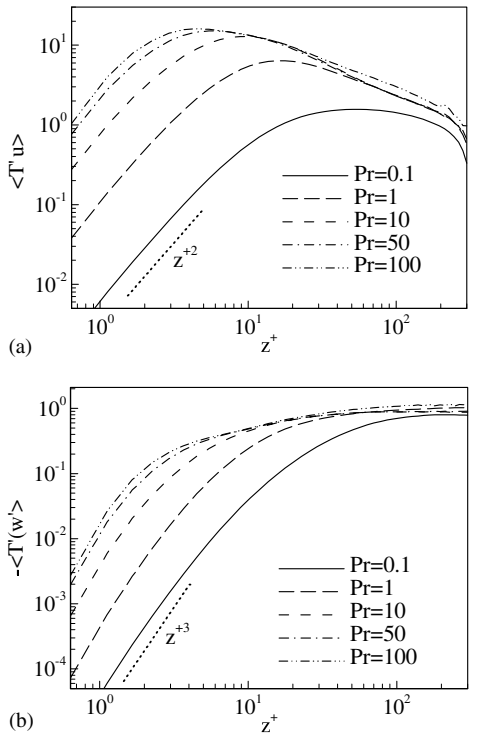

Fig. 7. Distributions of the mean streamwise and vertical turbulent heat fluxes at medium frequency: (a) streamwise turbulent heat flux; (b) vertical turbulent heat flux.

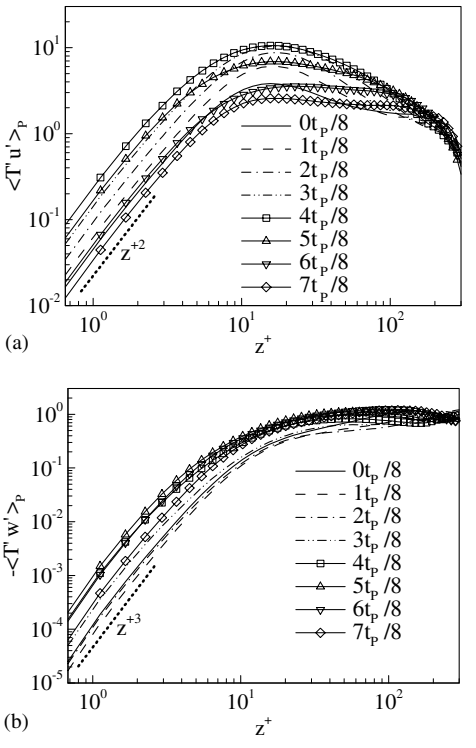

Fig. 8. Profiles of the phase-averaged streamwise and wall-normal turbulent heat fluxes for $Pr = 1$ at medium frequency: (a) streamwise turbulent heat flux; (b) vertical turbulent heat flux.

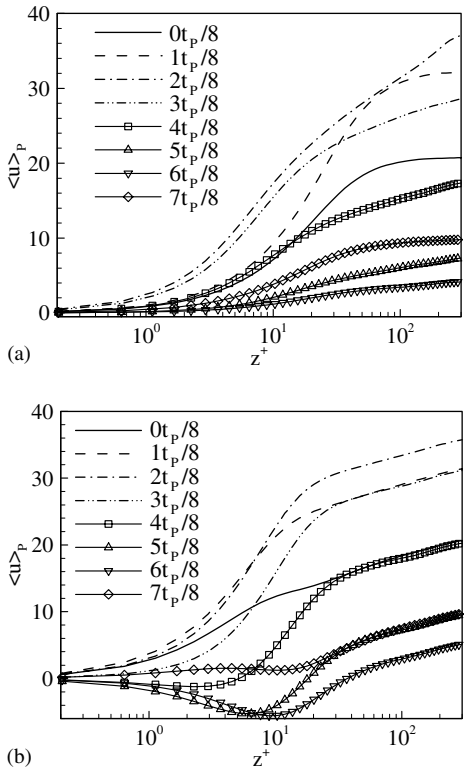

Fig. 9. Distributions of the phase-averaged velocity at several phases: (a) low frequency (case 1); (b) high frequency (case 3).

4.3. Effect of the driving frequency on turbulent flow and heat transfer

The phase-averaged quantities for low and high frequency, corresponding to case 1 and case 3, are briefly discussed. Fig. 9 shows the distributions of the phase-averaged velocity during the cycle for both low and high frequencies. At low frequency in Fig. 9a, the entire flow is strongly affected by the oscillation from the mean velocity profiles and the flow relaminarizes during the cycle with little residual turbulent fluctuations (not shown here). At high frequency in Fig. 9b, the mean velocity profile in the outer region remains essentially unaltered and a logarithmic layer with the usual slope is illustrated.

To reveal the effect of driving frequency on turbulent heat transfer, Figs. 10 and 11 show the phase-averaged temperature and its fluctuation, and the phase-averaged streamwise and wall-normal turbulent heat fluxes at $Pr = 1$ for low and high frequency. The corresponding quantities at medium frequency are shown in Figs. 4b, 6b and 8, respectively. As expected, at low frequency in Fig. 10, the difference of those quantities for different phases is obvious. However, at high driving frequency in Fig. 11, little difference is seen with respect to the statistically steady case. This behavior agrees well with previous numerical results [18,19] and experimental data [31,32]. Meanwhile, as shown in Figs. 10c,d and 11c,d the turbulent heat fluxes in the streamwise and

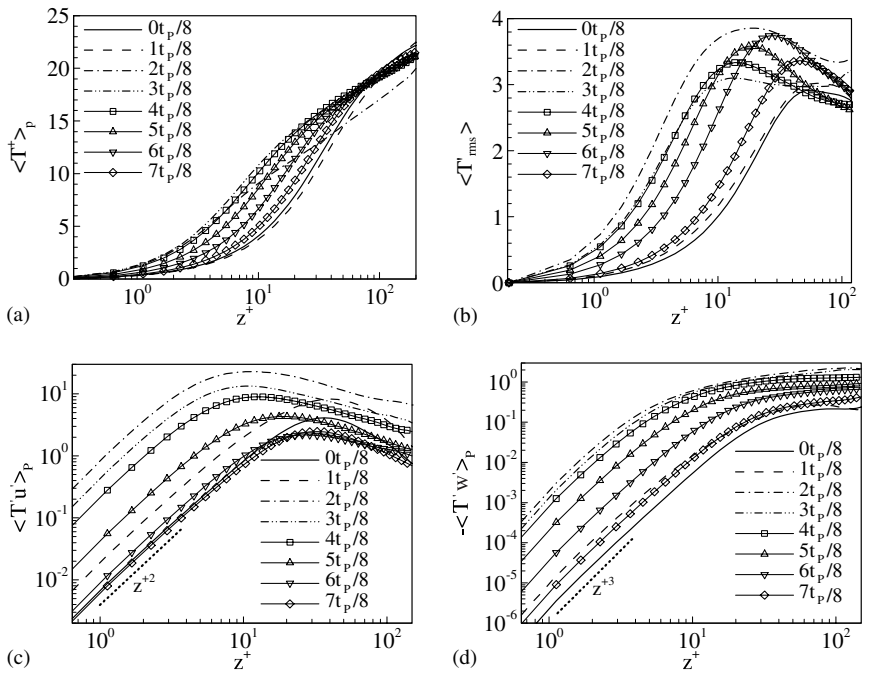

Fig. 10. Distributions of the phase-averaged quantities at low frequency (case 1): (a) temperature; (b) temperature fluctuation; (c) streamwise turbulent heat flux; (d) wall-normal turbulent heat flux.

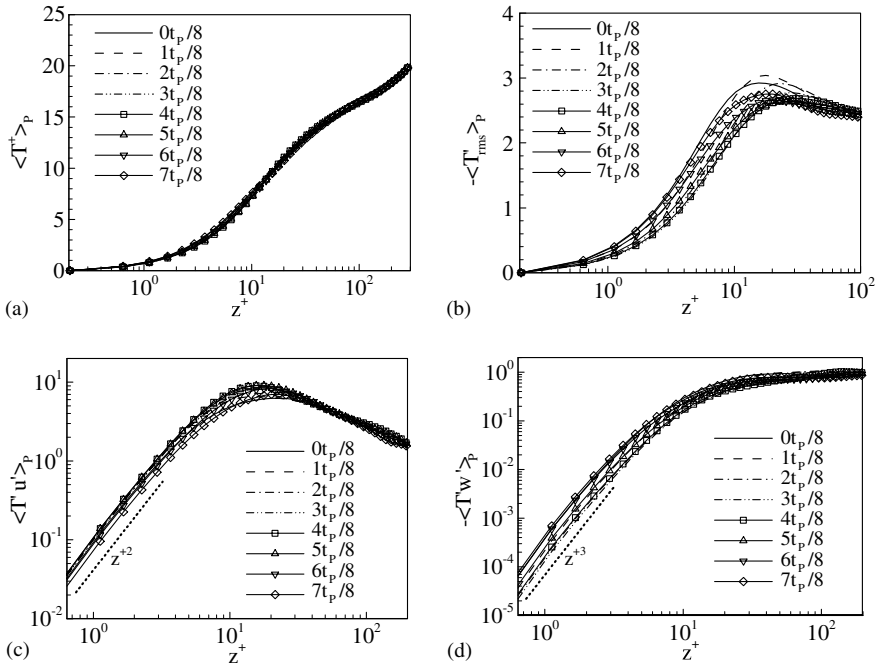

Fig. 11. Distributions of the phase-averaged quantities at high frequency (case 3): (a) temperature; (b) temperature fluctuation; (c) streamwise turbulent heat flux; (d) wall-normal turbulent heat flux.

wall-normal directions are consistent perfectly with the leading term behavior in (10) in the near wall region.

4.4. Turbulence structure

The effect of the oscillating flow on the turbulent statistics stems from a profoundly different topology of turbulent structures. The structures of instantaneous velocity and temperature fluctuations are briefly discussed to support the time evolution of the turbulent quantities described in the above. Fig. 12 shows the patterns of instantaneous streamwise velocity and temperature fluctuation in the (x, y) plane at $z^+ = 8$ for medium frequency (i.e., case 2). As the flow picks up momentum, very long and smooth streaks develop and burst into a localized turbulent spot in Fig. 12a, eventually fill the whole channel in Fig. 12b. Those streak-structures undergoing a spot-like transition were reported experimentally by Sarpkaya [33]. The corresponding instantaneous temperature fluctuation fields at $Pr = 1$ are shown in Fig. 12c and d. One can identify the local spots in accordance with the high- and low-temperature regions alternately. These visualizations imply that the turbulent mixing of temperature is controlled by the turbulence dynamics in the near wall region.

Contours of the resolved temperature fluctuation close to the wall in a cross plane (y, z^+) for $Pr = 1$, 10 and 100 at medium frequency are shown in Fig. 13, where the high- and low-temperature streaks are visualized. The organized streaks of the temperature fluctuation exhibit the coherent structures due to the succession of ejection and sweeping events. It is identified that smaller scale structures near the solid boundary appear at higher Prandtl number. The scale in the temperature fluctuation decreases with the increase of Prandtl number in a manner inversely proportional to $Pr^{1/2}$ indicated by Tennekes and Lumley [34]. The vertical size of the closed temperature contours clearly shows that the heat transfer takes place in a much thinner region at $Pr = 100$ than at $Pr = 1$. Consequently, nearly all the turbulent structures existing in the wall region are effective in the heat transfer process at $Pr = 1$, but only the smallest structures subsisting very close to the wall are involved in the transfer process at $Pr = 100$.

5. Concluding remarks

Large eddy simulation of an oscillating turbulent channel flow with heat transfer is performed for the Prandtl number from 0.1 up to 100 and the Reynolds number 350. The frequency of driving pressure gradient for the oscillating turbulent channel flow ranges low, medium and high values. Statistical turbulence quantities including the mean and phase-averaged velocity, temperature and their fluctuations, heat transfer coeffi-

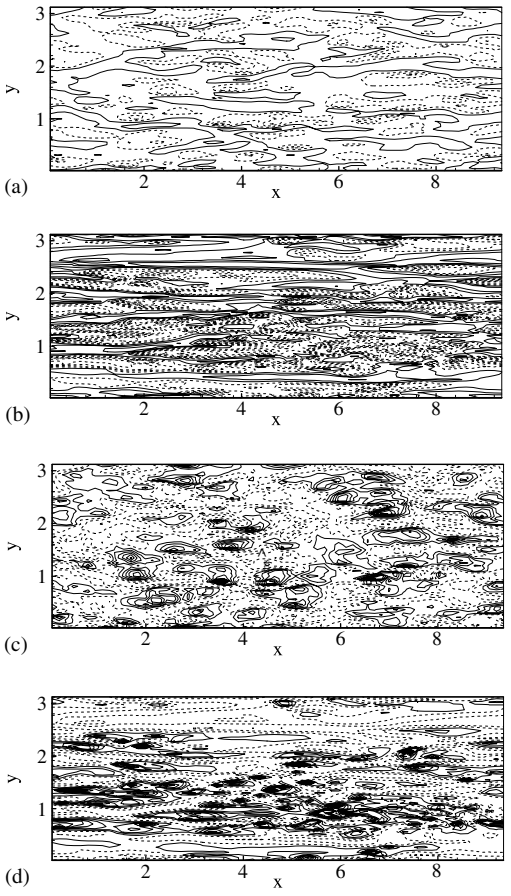

Fig. 12. Contours of instantaneous streamwise velocity fluctuation and temperature fluctuation in the (x, y) plane with $z^+ = 8$ at medium frequency (case 2): (a) streamwise velocity fluctuation at $0t_P/2$; (b) streamwise velocity fluctuation at $t_P/2$; (c) temperature fluctuation at $0t_P/2$; (d) temperature fluctuation at $t_P/2$.

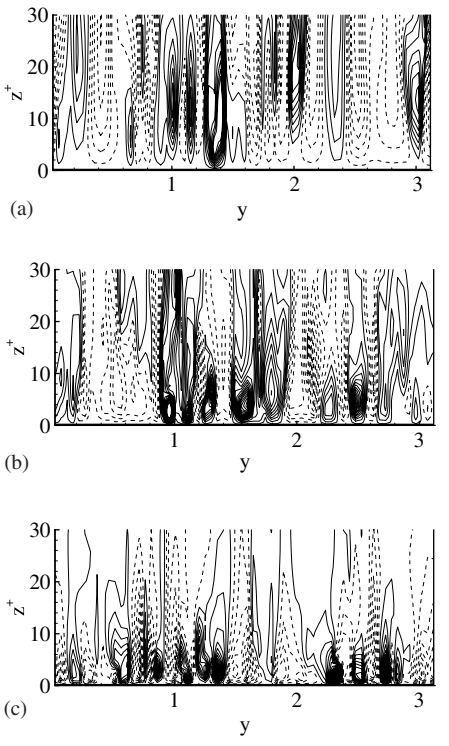

Fig. 13. Contours of instantaneous temperature fluctuation close to the wall in a cross plane (y, z^+) for different Prandtl numbers at medium frequency (case 2) at $t_P/2$: (a) $Pr = 1$; (b) $Pr = 10$; (c) $Pr = 100$.

cients, turbulent heat fluxes are obtained and analyzed. At high-Prandtl number, it has been established that the mean and phase-averaged quantities of the oscillating turbulent flow with heat transfer still obey reasonably those relations predicted theoretically or experimentally for fully developed statistically steady turbulent wall flow case. The mean diffusive sublayer thickness δ_T^+ and the mean (and phase-averaged) turbulent heat transfer coefficients K_T^+ (and K_{TP}^+) behave like $Pr^{-1/3}$ and $Pr^{-2/3}$ as proposed theoretically by Kader and Yaglom [26], or like $Pr^{-0.3}$ and $Pr^{-0.7}$ predicted experimentally by Shaw and Hanratty [28]. Based on the profiles of the mean and phase-averaged temperature and temperature fluctuation, there exists a buffer layer followed by a logarithmic region in the mean and phase-averaged temperature profiles. At low-Prandtl number, the temperature fluctuation is high in the whole channel except the wall region. However, at high-Prandtl number, the temperature fluctuation over the core region of the channel is negligibly small because the gradient of the mean temperature is nearly zero there. It is verified that the mean and phase-averaged streamwise and vertical turbulent heat fluxes vary in the manners of z^{+^2} and z^{+^3}, respectively, in the wall vicinity. Based on the structures of instantaneous temperature fluctuation contours, it is confirmed that the heat transfer takes place in a very thin region at high-Prandtl number and only the smallest structures subsisting very close to the wall are involved in the heat transfer process.

Acknowledgements

This work was supported by the National Science Fund for Distinguished Scholars (No. 10125210), the China NKBRSF Project (No. 2001CB409600), specialized Research Fund for the Doctoral Program of Higher Education (No. 20020358013), and the Programme of Hundred-Talent of the Chinese Academy of Sciences.

References

[1] J. Kim, P. Moin, Transport of passive scalars in a turbulent channel flow, in: J.-C. Andre et al. (Eds.), Turbulent Shear Flows, vol. 6, Springer-Verlag, Berlin, 1989, pp. 85–96.

[2] R.A. Antonia, J. Kim, Low-Reynolds number effects on near turbulence, J. Fluid Mech. 276 (1994) 61–80.

[3] N. Kasagi, Y. Tomita, A. Kuroda, Direct numerical simulation of passive scalar field in a turbulent channel flow, ASME J. Heat Transfer 144 (1992) 598–606.

[4] P.M. Wikström, A.V. Johansson, DNS and scalar-flux transport modelling in a turbulent channel flow, in: Proc. 2nd Conference Turbulent Heat Transfer, vol. 1, Manchester, UK, 1998, pp. 6.46–6.51.

[5] H. Kawamura, K. Ohsaka, H. Abe, K. Yamamoto, DNS of turbulent heat transfer in channel flow with low to medium-high Prandtl number fluid, Int. J. Heat Fluid Flow 19 (1998) 482–491.

[6] H. Kawamura, H. Abe, Y. Matsuo, DNS of turbulent heat transfer in channel flow with respect to Reynolds and Prandtl number effects, Int. J. Heat Fluid Flow 20 (1999) 196–207.

[7] Y. Na, D.V. Papavassiliou, T.J. Hanratty, Use of direct numerical simulation to study the effect of Prandtl number on temperature fields, Int. J. Heat Fluid Flow 20 (1999) 187–195.

[8] M. Germano, U. Piomelli, P. Moin, W. Cabot, A dynamic subgrid-scale eddy viscosity model, Phys. Fluids 3 (1991) 1760–1765.

[9] J. Smagorinsky, General circulation experiments with the primitive equations. I. The basic experiment, Mon. Weather Rev. 91 (1963) 99–165.

[10] W.-P. Wang, R.H. Pletcher, On the large eddy simulation of a turbulent channel flow with significant heat transfer, Phys. Fluids 8 (1996) 3354–3366.

[11] P. Moin, K. Squires, W. Cabot, S. Lee, A dynamic subgrid-scale model for compressible turbulent and scalar transport, Phys. Fluids 3 (1991) 2746–2757.

[12] Y. Zang, R.L. Street, J.R. Koseff, A dynamic mixed subgrid-scale model and its application to turbulent recirculating flows, Phys. Fluids 5 (1993) 3186–3196.

[13] N.Y. Liu, X.Y. Lu, L.X. Zhuang, A new dynamic subgrid-scale model for the large eddy simulation of stratified turbulent flows, Sci. China 43 (2000) 391–399.

[14] F.Q. Zhong, N.S. Liu, X.Y. Lu, L.X. Zhuang, An improved dynamic subgrid-scale model for the large eddy simulation of stratified channel flow, Sci. China 45 (2002) 888–899.

[15] Y.H. Dong, X.Y. Lu, L.X. Zhuang, Large eddy simulation of turbulent channel flow with mass transfer at high-Schmidt numbers, Int. J. Heat Mass Transfer 46 (2003) 1529–1539.

[16] P.R. Spalart, B.S. Baldwin, Direct simulation of a turbulent oscillating boundary layer, in: J.-C. Andre et al. (Eds.), Turbulent Shear Flows, vol. 6, Springer-Verlag, Berlin, 1989, pp. 417–440.

[17] X.Y. Lu, C. Dalton, J. Zhang, Application of large eddy simulation to an oscillating flow past a circular cylinder, ASME J. Fluids Eng. 119 (1997) 519–525.

[18] C.T. Hsu, X.Y. Lu, M.K. Kwan, LES and RANS studies of oscillating flows over a flat plate, ASCE J. Eng. Mech. 126 (2000) 186–193.

[19] A. Scotti, U. Piomelli, Numerical simulation of pulsating turbulent channel flow, Phys. Fluids 13 (2001) 1367–1384.

[20] R. Verzicco, P. Orlandi, A finite-difference scheme for three-dimensional incompressible flows in cylindrical coordinates, J. Comput. Phys. 123 (1996) 402–414.

[21] U. Piomelli, E. Balaras, Wall-layer models for large-eddy simulations, Annu. Rev. Fluid Mech. 34 (2002) 349–374.

[22] P. Moin, J. Kim, Numerical investigation of turbulent channel flow, J Fluid Mech. 118 (1982) 341–377.

[23] Y. Nagano, M. Shimada, Development of a two-equation heat transfer model based on direct simulations of turbulent flows with different Prandtl numbers, Phys. Fluids 8 (1996) 3379–3402.

[24] S. Tardu, G. Binder, R.F. Blackwelder, Turbulent channel flow with large-amplitude velocity oscillations, J. Fluid Mech. 267 (1994) 109–151.

[25] M. Hino, M. Kashiwayanagi, A. Nakayama, T. Hara, Experiments on the turbulence statistics and the structure of a reciprocating oscillatory flow, J. Fluid Mech. 131 (1983) 363–400.

[26] B.A. Kader, A.M. Yaglom, Heat and mass transfer laws for fully turbulent wall flows, Int. J. Heat Mass Transfer 15 (1972) 2329–2342.

[27] B.A. Kader, Temperature and concentration profiles in fully turbulent boundary layers, Int. J. Heat Mass Transfer 24 (1981) 1541–1545.

[28] D.A. Shaw, T.J. Hanratty, Turbulent mass transfer rates to a wall for large Schmidt number, AIChE J. 23 (1977) 28–35.

[29] S.L. Lyons, T.J. Hanratty, J.B. Mclaughlin, Direct numerical simulation of passive heat transfer in turbulent channel flow, Int. J. Heat Mass Transfer 34 (1991) 1149–1161.

[30] S.L. Lyons, T.J. Hanratty, J.B. Mclaughlin, Large-scale computer simulation of fully developed turbulent channel flow, Int. J. Numer. Meth. Fluids 13 (1991) 999–1028.

[31] G.J. Brereton, W.C. Reynolds, R. Jayaraman, Response of a turbulent boundary layer to sinusoidal free-stream unsteadiness, J. Fluid Mech. 221 (1990) 131–159.

[32] G.J. Brereton, W.C. Reynolds, Dynamic response of boundary-layer turbulence to oscillatory shear, Phys. Fluids A 3 (1991) 178–187.

[33] T. Sarpkaya, Coherent structures in oscillatory boundary layers, J. Fluid Mech. 253 (1993) 105–140.

[34] H. Tennekes, J.L. Lumley, A First Course in Turbulence, MIT Press, Cambridge, MA, 1972, pp. 95–97.